instruments

MDPI

Article

Geant4-Based Characterization of Muon, Electron, Photon, and Hadron Signals from Atmospheric Showers in a Water Cherenkov Detector

Luiz Augusto Stuani Pereira [1,2,*] and Raiff Hugo Santos [2]

[1] Instituto de Física, Universidade de São Paulo (IFUSP), R. do Matão, 1371, São Paulo 05508-090, SP, Brazil
[2] Unidade Acadêmica de Física, Universidade Federal de Campina Grande (UAF-UFCG), R. Aprígio Veloso, 882, Campina Grande 58429-900, PB, Brazil; raiff.hugo@estudante.ufcg.edu.br
* Correspondence: luizstuani@uaf.ufcg.edu.br

Abstract

Cherenkov radiation is a widely used detection mechanism in high-energy and astroparticle physics experiments, particularly in water-based detectors operated by leading cosmic-ray observatories. Its popularity stems from its robustness, cost-effectiveness, and high detection efficiency across a broad range of environmental conditions. In this study, we present a detailed Monte Carlo characterization of a Water Cherenkov Detector (WCD) using the Geant4 simulation toolkit as a general, experiment-independent reference for understanding detector responses to secondary cosmic-ray particles. The detector is modeled to register secondary particles produced by the interaction of high-energy cosmic-ray primaries with the Earth's atmosphere, which give rise to extensive air showers composed of hadronic, electromagnetic, and muonic components capable of reaching ground level. By simulating the differential energy spectra and angular distributions of these particles at the surface, we evaluate the WCD response in terms of energy deposition, Cherenkov photon production, photoelectron generation at the photomultiplier tube, and the resulting charge spectra. The results establish a systematic and transferable baseline for detector performance characterization and particle identification, providing a physically grounded reference that can support calibration, trigger optimization, and analysis efforts across different WCD-based experiments.

Keywords: Water Cherenkov Detector; extensive air showers; Geant4 simulation; secondary cosmic-ray particles; detector response characterization

check for updates

Academic Editor: Martin Pohl

Received: 1 October 2025
Revised: 11 November 2025
Accepted: 21 November 2025
Published: 24 November 2025

Citation: Stuani Pereira, L.A.; Santos, R.H. Geant4-Based Characterization of Muon, Electron, Photon, and Hadron Signals from Atmospheric Showers in a Water Cherenkov Detector. *Instruments* **2025**, *9*, 28. https://doi.org/10.3390/instruments9040028

Copyright: © 2025 by the authors. Licensee MDPI, Basel, Switzerland. This article is an open access article distributed under the terms and conditions of the Creative Commons Attribution (CC BY) license (https://creativecommons.org/licenses/by/4.0/).

1. Introduction

Cosmic rays are high-energy particles originating from outer space that continuously bombard the Earth's atmosphere [1,2]. When these primary cosmic rays, mainly protons and heavier nuclei, interact with atmospheric nuclei, they produce cascades of secondary particles in a process known as an extensive air shower [3]. These showers contain a variety of particles, including muons, electrons, photons, and hadrons, which can reach ground level depending on their energy and the altitude of the observation site [4]. The study of these secondary particles provides valuable insights into the nature and origins of cosmic radiation, as well as fundamental processes in high-energy astrophysics and particle interactions in the atmosphere [5]. Detecting and characterizing these particles requires specialized instrumentation capable of capturing their signatures with high efficiency and precision.

Among the instruments used to detect secondary cosmic-ray particles, Water Cherenkov Detectors (WCDs) stand out due to their high efficiency in identifying the signals produced by these particles [6]. This efficiency, combined with their relatively low cost, has led to WCDs being widely adopted in astroparticle physics experiments. Notable examples include INCA in Chacaltaya, Bolivia (5200 m a.s.l.) [7]; Milagro in New Mexico, USA (2650 m a.s.l.) [8]; the Pierre Auger Observatory in Malargüe, Argentina (1400 m a.s.l.) [9]; the HAWC (High-Altitude Water Cherenkov Observatory) in Sierra Negra, Mexico (4500 m a.s.l.) [10]; the LHASSO (Large High-Altitude Air Shower Observatory) in Sichuan, China (4410 m a.s.l.) [11]; and the Latin American Giant Observatory (LAGO), distributed across Latin America [12].

In these detectors, water serves as the dielectric medium for generating Cherenkov radiation. When high-energy charged particles pass through water at speeds exceeding the phase velocity of light in the medium, they emit Cherenkov photons. These photons are detected by photomultiplier tubes (PMTs) positioned inside the tank [13,14]. The design of the detector can vary depending on the experimental objectives, allowing optimization for specific particle types or energy ranges [15]. PMTs operate by converting incoming Cherenkov photons into photoelectrons via the photoelectric effect. These photoelectrons are then accelerated and amplified through a cascade of dynodes, generating measurable electric pulses [16]. This amplification process enables the detection of even faint Cherenkov signals, making the WCD highly effective in registering the passage of relativistic particles.

To improve light collection efficiency, the interior walls of the detector tanks are often lined with reflective materials, such as Tyvek. Due to its high reflectivity and durability, Tyvek enhances the redirection of Cherenkov photons toward the PMTs, thereby reducing light losses and improving the overall sensitivity of the detector [17].

Beyond their ability to detect charged secondary particles, WCDs are also effective in identifying high-energy photons from cosmic radiation through an indirect mechanism [18]. Primary photons above the pair-production threshold ($>$1.022 MeV) convert into electron–positron pairs ($e^{\pm}$) in the water volume, with particularly high conversion probability in one cubic meter of water [19]. These secondary $e^{\pm}$ pairs then emit Cherenkov radiation, which is detected by the PMTs. Furthermore, the versatility of WCDs has recently been expanded to include neutron detection [20–22], opening new possibilities for their application across a broader range of scientific investigations, including nuclear monitoring and space weather studies.

Given the versatility and widespread adoption of WCDs in astroparticle physics, a deeper understanding of the distinct signals produced by different secondary particles is essential for improving detection performance and interpretation accuracy. A fundamental challenge in WCD-based experiments is particle identification and discrimination. Unlike tracking detectors or imaging calorimeters, WCDs are inherently non-imaging detectors that provide limited observables, primarily charge (or photon count) and timing information, from which particle type, energy, and multiplicity must be inferred. This presents several practical challenges: distinguishing electromagnetic showers from single muons (critical for gamma-ray astronomy), identifying hadron contributions to understand shower composition, accounting for neutron backgrounds, and optimizing trigger thresholds that balance detection efficiency against noise. Addressing these challenges requires a detailed quantitative understanding of how each particle species interacts with the detector and translates into measurable signals.

While major experiments such as Pierre Auger [9], the HAWC [10], and others have developed sophisticated detector simulations tailored to their specific configurations and scientific goals, the literature still lacks a comprehensive and standardized comparison of WCD responses to all major secondary particle species within a single, unified simulation and analysis framework. This work addresses that gap by systematically investigating the characteristic interactions and detector responses of muons, electrons/positrons, photons,

protons, and neutrons in a reference WCD model using open-source tools. The novelty of this study lies in its role as a general, experiment-independent benchmark that isolates the physical processes shaping WCD observables—energy deposition, Cherenkov photon production, and PMT signal formation—under controlled and reproducible conditions. By providing a quantitative comparison of these responses, this study establishes a physically grounded reference that can inform particle-identification algorithms, trigger optimization, and detector calibration across a range of WCD-based experiments and prototype designs.

The rest of this paper is organized as follows: Section 2 presents the simulation methodology, detailing the two-stage framework based on the Cosmic-Ray Shower Generator and the Geant4 Monte Carlo toolkit. Section 3 discusses the simulation results, focusing on the detector's response to the different particle species. Finally, Section 4 summarizes the main findings and highlights their implications for particle identification in WCDs.

2. Materials and Methods

To investigate the response of the WCD to secondary particles from extensive air showers, a two-stage simulation framework was implemented. First, secondary particles at the ground level were generated using the CRY (Cosmic-Ray Shower Generator) toolkit [23], which provides realistic particle fluxes based on empirical cosmic-ray spectra. In the second stage, the interactions of these particles within the WCD were modeled using the Geant4 Monte Carlo simulation toolkit. This framework allows for a detailed analysis of energy deposition, Cherenkov photon production, and signal formation in the photomultiplier tube. The following subsections describe the configuration and use of both CRY and Geant4 [24] in this study.

2.1. CRY—Cosmic-Ray Shower Generator

CRY is a software library that generates secondary particle distributions from cosmic ray-induced atmospheric showers at various altitudes (sea level, 2100 m, and 11,300 m a.s.l.) for use in detector simulations. It relies on pre-computed tables from MCNPX simulations of primary cosmic-ray interactions with the atmosphere, showing good agreement with experimental data [25]. CRY provides fluxes of muons, neutrons, protons, electrons, photons, and pions within user-defined areas and altitudes, sampling their energy, arrival time, zenith angle, and multiplicity. It supports geomagnetic cut-off and solar cycle effects, and it can be integrated into C, C++, Fortran, and Monte Carlo frameworks, such as Geant4.

Unlike CORSIKA [3], which performs full Monte Carlo simulations of air shower development from primary cosmic-ray interactions to ground level, CRY provides pre-computed particle distributions at fixed altitudes based on MCNPX calculations. While CORSIKA offers greater flexibility in primary particle types, energy ranges (up to 10^{20} eV), and site-specific atmospheric profiles, CRY's lookup-table approach significantly reduces computational overhead and is well suited for detector-level response studies where detailed shower development is not required. For the present work, which focuses on characterizing the WCD response to secondary particles at sea level (1 GeV–100 TeV primary energy range), CRY provides realistic input distributions with sufficient accuracy at a much lower computational cost [23,25].

The primary cosmic rays used in the CRY simulation are protons with energies ranging from 1 GeV to 100 TeV, which are injected at the top of the atmosphere. The atmosphere was modeled as a series of 42 flat density layers, each composed of 78% N_2, 21% O_2, and 1% Ar by volume. The density change between adjacent layers was set at 10%, with values derived from the 1976 U.S. Standard Atmosphere model. The top of the atmosphere is located at an altitude of approximately 31 km, with an integrated column density of about 1000 g/cm^2 [23].

In this work, the distribution of secondary cosmic-ray particles at sea level was used, corresponding to the latitude of Campina Grande, Paraíba, Brazil (7.2206° S). This latitude was randomly chosen for this study and could be replaced by that of any other city worldwide. The latitude was employed to adjust the primary cosmic-ray spectrum by accounting for the geomagnetic field. Additionally, a specific date (in month–day–year format) was set to adjust the cosmic ray spectrum according to the 11-year solar cycle [26]. The solar cycle, also known as the solar magnetic activity cycle, is an approximately 11-year periodic variation in solar activity, measured by changes in the number of sunspots observed on the solar surface. During periods of high solar activity, the Sun's emissions of matter and electromagnetic fields increase, making it more difficult for galactic cosmic rays to reach Earth. Consequently, cosmic-ray intensity is lower when solar activity is high.

In this study, the CRY generator was configured for 16 September 2025, corresponding to the ascending phase of solar cycle 25, near the expected solar maximum.

Figures 1 and 2 display the event-count distributions of incident energy (events per logarithmic bin) and zenith angle (events per bin), with θ expressed in degrees. For cross-species comparability, we use shared binning—energy in 60 logarithmic bins spanning the data range with a 5% margin, and θ in 72 linear bins over 0°–180°. A support-aware Gaussian smoothing curve (reflective padding; no extrapolation beyond populated bins) is overlaid purely to guide the eye, and the legends report the corresponding mean values. Based on these distributions, muons are the most energetic particles reaching the ground, while the electromagnetic component (electrons and photons) dominates in abundance at the detector level, followed by muons and then hadrons (protons and neutrons).

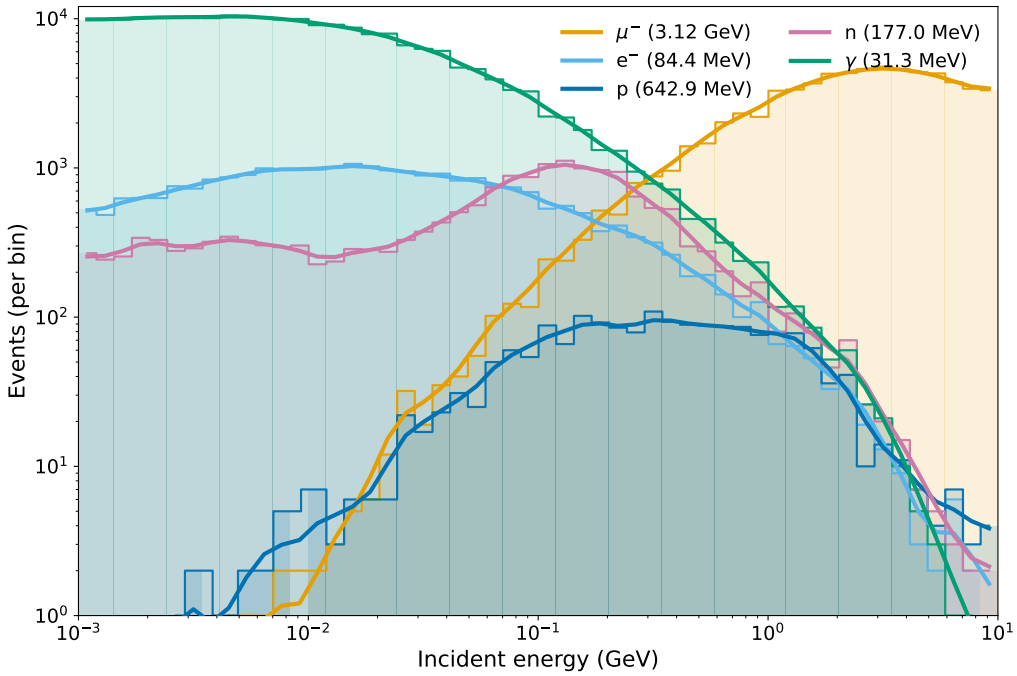

Figure 1. Incident-energy event-count distribution (events per bin) for secondary cosmic-ray particles interacting with the Water Cherenkov Detector. The energy range has been restricted to 1 MeV–10 GeV, corresponding to the interval relevant for Cherenkov light production in the WCD volume; higher-energy components from the CRY source distributions are omitted for clarity, as they lie outside the detector's effective operational range. Histograms use shared logarithmic binning (52 bins spanning 1.3 decades) and are shown on log–log axes with logarithmic vertical scaling to visualize low-statistics species. A Gaussian smoothing curve (with reflective padding and no extrapolation beyond unpopulated bins) is overlaid for visualization only. The mean values shown in the legend are provided solely as reference points for cross-species comparison and are not used for quantitative analysis.

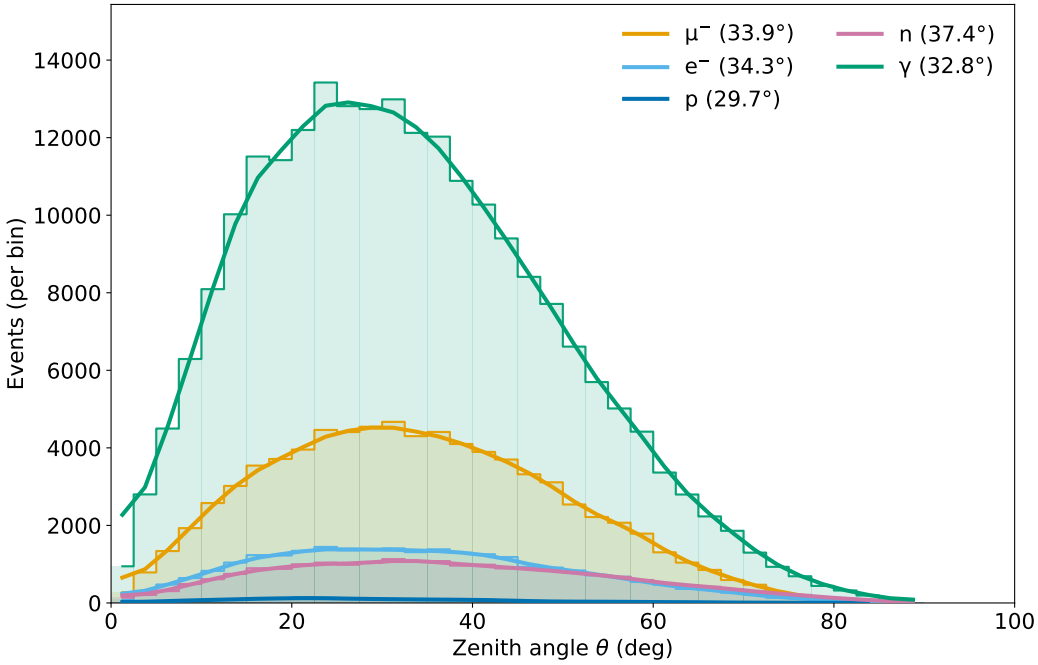

Figure 2. Zenith–angle event–count distribution (events per bin) for secondary cosmic–ray particles interacting with the Water Cherenkov Detector, with θ expressed in degrees. Histograms use shared linear bins (72 bins over 0°–180°); a Gaussian smoothing curve (with reflective padding and no extrapolation beyond unpopulated bins) is overlaid for visualization only; mean angles are indicative and not used for statistical inference.

The low-energy cut-offs visible near 1 MeV for electrons and photons correspond to the lower limit of the CRY-generated secondary spectra at sea level, which exclude sub-MeV components outside the generator's validated energy range. These apparent thresholds are therefore intrinsic to CRY's source tables rather than artificial cuts applied in our analysis.

The neutron spectrum generated by the CRY toolkit extends into the sub-eV region, reflecting the presence of thermalized neutrons resulting from atmospheric and ground-level moderation. These low-energy neutrons were retained in the simulation for completeness and to maintain consistent normalization across particle species. Although they do not contribute directly to Cherenkov emission, they can interact through elastic scattering and capture processes, producing secondary gamma rays that are relevant for background characterization in Water Cherenkov Detectors.

2.2. Monte Carlo Simulation Framework Using Geant4

The geometry of the Water Cherenkov Detector (WCD) was implemented using the Geant4 simulation toolkit. Geant4 (GEometry ANd Tracking 4) (https://geant4.web.cern.ch/ (accessed on 15 September 2025)) is a widely used platform for simulating the interactions of electromagnetic and hadronic radiation with matter. In this work, the detector was modeled as a cylindrical structure with a diameter of 3.6 m and a total height of 2.1 m, containing a 1.9 m water column, corresponding to a total water volume of approximately 19.3 m^3. A single 8-inch Hamamatsu photomultiplier tube (PMT) was positioned at the center of the tank's bottom, with its photocathode facing upward to collect Cherenkov photons produced in the water volume. The PMT quantum efficiency (QE $\approx$ 25% at 400 nm) and nominal gain (G $\approx 10^7$) were adopted following the typical operational parameters of the Hamamatsu R5912 tubes used in the LAGO WCDs [9,17]. This single-PMT configuration represents a fully filled and stable tank, neglecting evaporation losses. The tank's inner cavity is enclosed by a polyethylene wall, which is internally lined with Tyvek, a highly reflective material that enhances Cherenkov photon collection. Secondary

particles generated by CRY were injected uniformly over the top surface of the detector, with their energies, zenith angles, and particle types sampled according to the distributions described in the previous section. This configuration enables a detailed and consistent simulation of particle interactions within the medium, offering precise control of physical parameters and ensuring the reproducibility of the results. Moreover, the model allows for straightforward adjustments to geometry and material properties, facilitating performance studies and future optimization.

As previously mentioned, all simulations involving the transport and interaction of cosmic radiation within the Water Cherenkov Detector were carried out using the Geant4 toolkit. To model hadronic interactions within the detector medium, the simulations employed the `QGSP_BERT_HP` reference physics list. This configuration combines the quark–gluon string model (QGSP) to describe nucleon and pion interactions above approximately 15 GeV with the Bertini intra-nuclear cascade model (BERT) for lower incident energies, ensuring a realistic treatment of secondary interactions in light materials such as water. The `_HP` suffix denotes the High-Precision `NeutronHP` extension, which incorporates evaluated cross-section data from the `ENDF/B-VII.1` library to accurately simulate neutron elastic and inelastic scattering below 20 MeV, an essential consideration for modeling capture gamma-ray production and other background processes in water-based detectors. Electromagnetic processes involving charged particles, gamma rays, and optical photons (including Cherenkov light) were handled using the `G4EmStandardPhysics` and `G4OpticalPhysics` packages, which are the recommended constructors for high-energy and optical simulations [27]. Together, these configurations ensure the accurate treatment of both primary and secondary particles, as well as the realistic generation, propagation, and detection of Cherenkov radiation within the detector volume.

3. Results and Discussion

This section presents the simulation results for the WCD response to secondary particles generated in atmospheric showers. The analysis focuses on the key physical processes that govern the detector's performance. First, we examine the energy-deposition profiles of muons, electrons, photons, and hadrons within the water volume to assess their respective contributions to the overall detector signal. Next, we analyze the generation and spatial distribution of Cherenkov photons arising from these energy depositions, providing insight into the light yield associated with each particle type. Finally, we investigate the propagation of Cherenkov photons to the photomultiplier tube (PMT), with emphasis on photoelectron production and the resulting charge spectra. Together, these results provide a comprehensive characterization of the WCD's capability to detect and distinguish between different secondary particles in extensive air showers.

3.1. Energy Deposition of Secondary Particles in the WCD

The distributions of energy deposited by secondary particles in the WCD were evaluated through Monte Carlo simulations. In this context, the deposited energy is defined as the total energy lost by a particle within the water volume of the detector, as recorded by Geant4 at each simulation step. This includes all microscopic losses resulting from ionization (the dominant process for charged particles), Compton scattering, pair production, and hadronic interactions, depending on the particle type. These deposited-energy values represent the cumulative energy transferred to the medium per event, excluding energy carried away by escaping particles or secondary photons that do not reinteract within the detector. The analyzed particles—muons, electrons, photons, and hadrons—originate from extensive air showers initiated by high-energy primaries and collectively define the detector's response to the main components of secondary cosmic radiation.

Figure 3 shows the event-count distributions of deposited energy (events per logarithmic bin) for the main secondary particle species, constructed with shared logarithmic binning across species and smoothed with a Gaussian filter for visualization. Since the vertical axis reports raw event counts per bin, the amplitudes encode both the relative abundance of each species at the detector level and the underlying sample statistics. The mean deposited energies are approximately 0.40 GeV for muons, 0.11 GeV for electrons, 0.03 GeV for photons, 0.59 GeV for protons, and 0.12 GeV for neutrons.

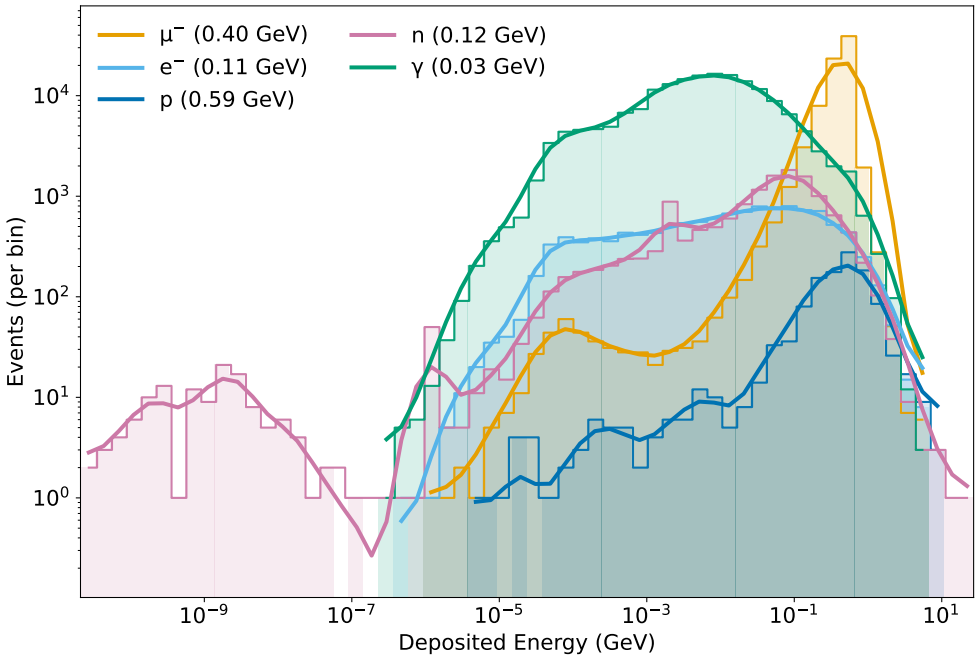

Figure 3. Deposited-energy event-count distributions in the WCD: events per logarithmic bin (log–log axes) versus deposited energy (GeV) for secondary muons, electrons, photons, protons, and neutrons. Shared logarithmic binning across species (60 bins with a 5% margin) is used. The Gaussian smoothing overlay serves for visualization only. The mean deposited-energy values indicated in the legend are descriptive, not inferential.

Electrons and photons dominate the low-energy region, where energy loss is governed by ionization, Compton scattering, and pair production, in agreement with standard electromagnetic shower physics [2,28]. Protons exhibit a broader distribution with a higher mean (0.59 GeV), reflecting occasional inelastic nuclear interactions that transfer substantial energy to the medium [4,29]. Muons, which typically behave as minimum-ionizing particles, present an intermediate mean (0.40 GeV). Their distribution, however, reveals a two-hump structure: a smaller peak centered near 10^{-4} GeV, corresponding to short or grazing trajectories that deposit only limited energy before exiting the detector; and a larger peak around 1 GeV, associated with through-going tracks that release nearly constant energy along the full water depth, consistent with observations reported in Auger and HAWC WCD studies [9,30].

Neutrons also display a two-band structure in their energy-deposition spectra. A lower band is centered near 10^{-9} GeV, reflecting low-energy recoil protons from single elastic scattering on hydrogen, while a more prominent band emerges around 10^{-1} GeV, linked to capture-induced γ emission and subsequent pair-production processes. Similar neutron capture signatures have been identified in underground and surface detector simulations [21,22,24,31]. These dual features illustrate the distinctive character of neutron interactions, which combine elastic scattering with secondary photon production mechanisms.

Taken together, these results indicate that while electromagnetic secondaries dominate at low deposited energies due to their abundance, muons and hadrons contribute larger per-event energy deposits, with muons and neutrons exhibiting unique multi-peaked structures that enhance their potential for discrimination in WCD-based analyzes.

The spectral features observed in Figure 3 are consistent with the interaction models implemented in the `QGSP_BERT_HP` physics list used in the Geant4 simulations. In this configuration, the Bertini intra-nuclear cascade model accurately reproduces secondary production and inelastic collisions of hadrons within light materials such as water, while the High-Precision (HP) extension governs the transport and capture of low-energy neutrons using evaluated `ENDF/B-VII.1` cross-sections down to the thermal range.

This comprehensive treatment explains the presence of the low-energy tail and the capture-induced peaks in the neutron spectra, as well as the realistic energy-deposition profiles obtained for all species. Although thermal neutrons contribute negligibly to Cherenkov emission, their inclusion ensures the proper modeling of delayed-capture gamma-ray backgrounds and enhances the overall physical fidelity of the detector response.

3.2. Cherenkov Photon Production by Secondary Particles in the WCD

The production of Cherenkov photons in the WCD is a fundamental process that directly determines the detector's ability to register and identify relativistic secondary particles from extensive air showers. Using detailed Monte Carlo simulations in a 1.90 m water column, we evaluated the photon yields for muons, electrons, photons, protons, and neutrons.

Figure 4 presents the event-count distributions of Cherenkov photon multiplicity N_{ch} (events per logarithmic bin) for the five species, adopting the same plotting conventions as in the deposited-energy distributions: shared logarithmic binning, log–log axes, and Gaussian smoothing overlaid only to guide the eye. Because the ordinate reports raw counts per bin, amplitudes encode both the relative abundance of particles at the detector level and the simulation statistics, while the curve shapes reflect the underlying production mechanisms and effective path lengths in water. The legend lists the mean multiplicities $\langle N_{\mathrm{ch}} \rangle$ for each species.

The observed species-dependent features are consistent with expectations for Water Cherenkov Detectors. Muons, with long above-threshold tracks, produce the most extended high-N_{ch} tail, reflecting their role as efficient Cherenkov emitters. Electrons and positrons, being lighter, experience stronger multiple scattering and shower development; they populate the lower-to-intermediate N_{ch} range but contribute substantially to the overall light yield due to their high abundance at sea level [2,5,13,24]. Photons, though neutral, contribute indirectly: above 1.022 MeV, they undergo pair production, generating $e^{\pm}$ that emit Cherenkov light as they propagate [4,14]. For primary photons at GeV-TeV energies, the resulting electromagnetic cascades produce substantial Cherenkov signals, making WCDs effective for gamma-ray astronomy at these energy scales, as demonstrated by Pierre Auger and HAWC observations [9,10].

This indirect detection mechanism is particularly pronounced for high-energy cosmic photons, which initiate extensive electromagnetic cascades in the atmosphere before reaching the detector.

High-energy primary photons interact predominantly in the upper atmosphere via pair production and subsequent bremsstrahlung processes, generating extensive air showers composed primarily of leptons (electrons and positrons) and secondary photons [2,4,9]. These secondary leptons, rather than the primary photon itself, constitute the main component reaching ground level and penetrating the WCD volume, where they exceed the Cherenkov threshold ($\beta > 1/n \approx 0.75$ in water) and emit radiation along their paths [13,14].

Within the tank, some of these relativistic leptons further undergo bremsstrahlung, producing high-energy photons that can convert into additional $e^{\pm}$ pairs through pair production, thereby extending the electromagnetic cascade inside the detector medium [18,19]. The resulting Cherenkov light yield thus arises from this coupled sequence of atmospheric and in-tank interactions: initial pair production in air, lepton traversal, and emission, followed by secondary bremsstrahlung and pair conversion, rather than direct photon absorption. This multi-stage process explains the characteristic N_{ch} distributions for photon-initiated events observed in Figure 4, consistent with electromagnetic shower development models validated in ground-level observations [2,9,10,13].

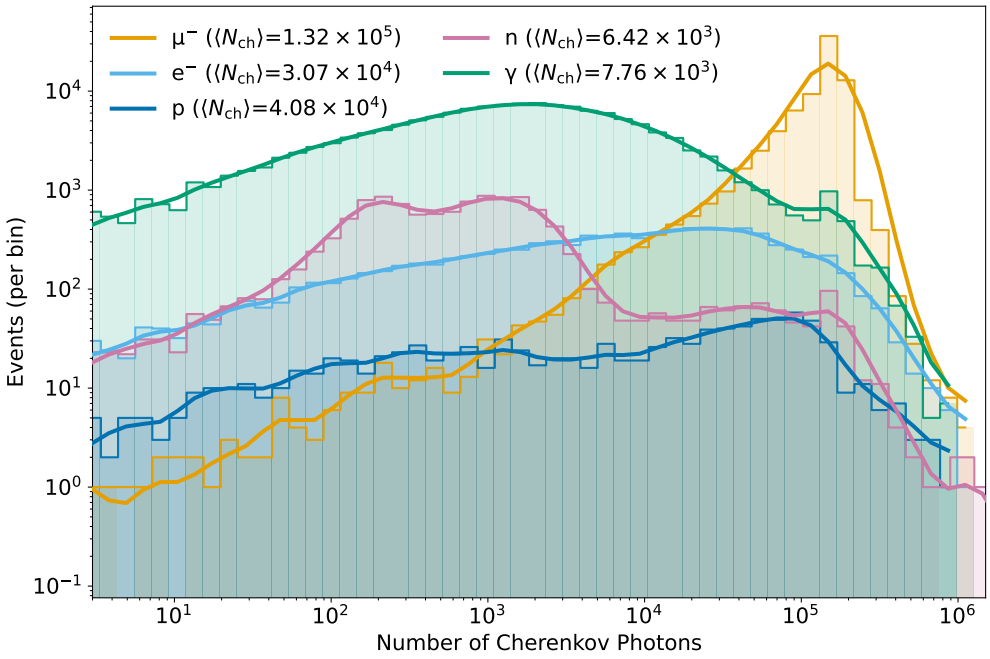

Figure 4. Cherenkov–photon multiplicity distributions in the WCD: event counts per logarithmic bin (log–log axes) of N_{ch} for secondary muons, electrons, photons, protons, and neutrons (1.90 m water column). Histograms use shared logarithmic binning across species; a support-aware Gaussian smoothing curve (reflective padding; no extrapolation beyond populated bins) is overlaid for visualization only. Legend entries report the mean photon counts $\langle N_{\mathrm{ch}} \rangle$, and amplitudes reflect the number of events in each energy interval.

Hadrons interact primarily through nuclear processes. Charged hadrons, especially protons, can emit Cherenkov photons once their kinetic energy exceeds the water threshold of ∼480 MeV ($\beta \approx 0.75$). The yields scale with both track length and velocity [6,13,14,27]. In our simulations, only a fraction of secondary protons arrives above the threshold, leading to photon production that is systematically lower than that for relativistic muons due to their shorter average path lengths and lower velocities [9]. Neutrons, in contrast, do not radiate directly but contribute through charged recoil secondaries produced in elastic and inelastic interactions, as well as via capture γ rays that convert into $e^{\pm}$ pairs [18–20,22]. Similar neutron-induced contributions have been reported in Auger and HAWC detectors [9,10]. Finally, the Tyvek lining of the inner walls enhances light collection by diffusively reflecting photons toward the PMT, thereby improving the detection probability. This effect is particularly relevant for low-yield cases, such as photon- and neutron-induced events. Overall, the N_{ch} distributions highlight the WCD's efficiency across multiple particle species and confirm the usefulness of photon-yield-based observables for particle discrimination in ground-based cosmic-ray experiments.

3.3. Photoelectron Production and Charge Response in the PMT

The response of the photomultiplier tube (PMT) provides the final observable link between the energy deposited in the WCD and the measurable electronic signal. After being produced in the water volume, Cherenkov photons propagate toward the PMT, where they may convert to photoelectrons with a probability set by the photocathode quantum efficiency (QE). In the present simulation, a single upward-facing Hamamatsu PMT was placed at the center of the tank bottom, following the configuration adopted in the Auger and LAGO detectors. The PMT was modeled with a quantum efficiency of $QE = 0.25$ in the 300–600 nm Cherenkov band and a gain of $G = 10^7$, representative of typical bialkali photomultipliers used in astroparticle physics [13,16]. Each photoelectron is subsequently multiplied through the dynode chain, producing an anode charge pulse proportional to the number of detected photons. This simplified yet realistic PMT model allows for a direct mapping between the optical photon statistics and the electronic observables while preserving reproducibility and general applicability across WCD configurations.

Two complementary observables capture this response: the number of Cherenkov photons reaching the PMT window (N_{hit}) and the integrated anode charge (Q). Figure 5 presents the event-count distributions of N_{hit} for secondary muons, electrons/positrons, photons, protons, and neutrons, following the same conventions as in the deposited-energy spectra. The mean values are $\langle N_{\text{hit}} \rangle \approx 2.55 \times 10^2$ for muons, 8.08×10^1 for electrons, 3.03×10^1 for photons, 1.41×10^2 for protons, and 2.43×10^1 for neutrons. As expected from their extended above-threshold tracks, muons display the broadest distribution and the most extended high-N_{hit} tail. Their spectrum exhibits a two-hump structure, with a smaller bump at low photon counts corresponding to partially contained or short-path events, and a larger bump at high counts associated with through-going muons that deposit nearly constant energy along the full tank depth. This dual structure parallels the two-band pattern already noted in the deposited-energy spectra, underlining the consistency of muon behavior across all observables. Electrons and positrons, strongly scattered and prone to electromagnetic cascades, populate the lower-to-intermediate region, while photons contribute indirectly through pair production above 1.022 MeV [4,10,14]. Protons contribute only when above the ∼480 MeV Cherenkov threshold [6,14], and neutrons yield the lowest averages, consistent with their indirect energy-deposition channels via recoil protons and capture γ rays [20,22].

Since the anode charge (Q) is linearly proportional to the number of detected photons (N_{hit}) through the PMT relation

$$Q\ [\text{pC}] \;=\; N_{\text{hit}} \times QE \times G \times e \times 10^{12},$$

where $QE = 0.25$, $G = 10^7$, and $e = 1.6022 \times 10^{-19}$ C, the two observables are physically equivalent up to a constant factor. Accordingly, only the N_{hit} distributions are shown, while the corresponding charge values are reported in the text for completeness. Numerically, this expression reduces to

$$Q \;\simeq\; N_{\text{hit}} \times 0.4005\ \text{pC},$$

yielding mean charges of $\langle Q \rangle \approx 1.02 \times 10^2$ pC for muons, 3.23×10^1 pC for electrons, 1.21×10^1 pC for photons, 5.65×10^1 pC for protons, and 9.74 pC for neutrons.

The double-hump pattern observed for muons in N_{hit}, and therefore also in Q, reflects the coexistence of short, partially contained tracks and fully through-going events. Electrons and photons cluster at lower values, protons occupy an intermediate range, and neutrons produce the lowest charges, consistent with their indirect Cherenkov contribution through recoil and capture processes. This proportionality confirms that the anode charge

distributions provide no additional independent information beyond the photon statistics already represented in Figure 5.

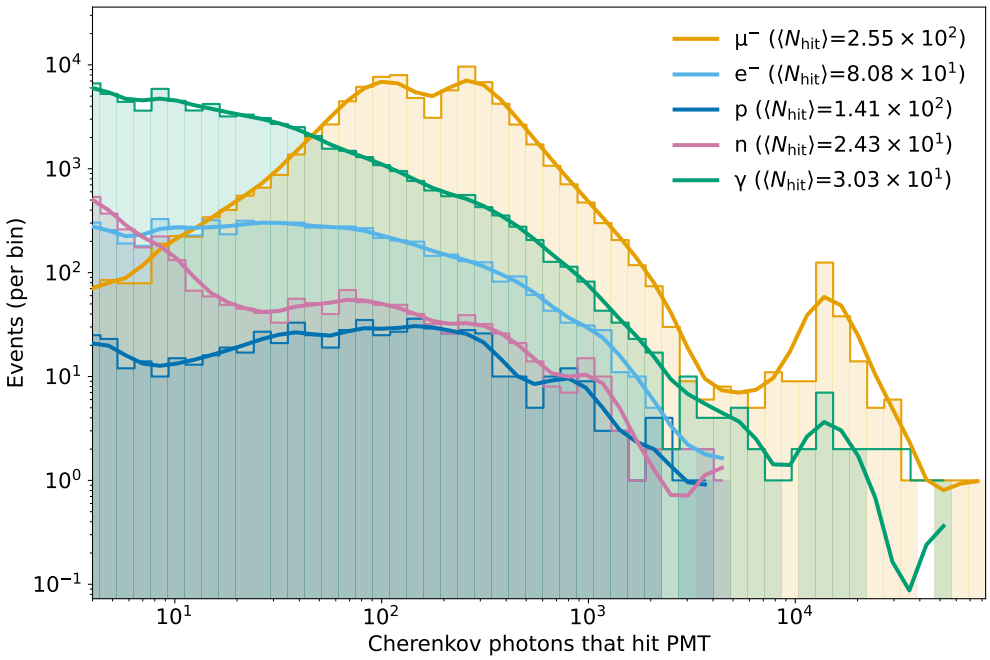

Figure 5. Cherenkov–photon HitCount at the PMT: event-count distributions (events per logarithmic bin; log–log axes) of N_{hit} for secondary muons, electrons/positrons, photons, protons, and neutrons (1.70 m water column). Histograms use shared logarithmic binning across species; a support-aware Gaussian smoothing (reflective padding; no extrapolation beyond populated bins) is overlaid for visualization only. Legend entries report the mean values $\langle N_{\mathrm{hit}} \rangle$; amplitudes reflect the number of events in each N_{hit} interval.

These results highlight the direct chain linking energy deposition → Cherenkov photon production → photon collection at the PMT → measured charge. The agreement between the species-dependent features in deposited energy, photon multiplicity, and PMT charge underscores the robustness of the simulation framework. Moreover, the explicit PMT modeling described here provides a reproducible and generalizable framework that can be adapted to other WCD configurations, facilitating cross-experiment comparisons and supporting the development of particle-identification and trigger algorithms in large-scale cosmic-ray observatories.

4. Conclusions

This work presents a detailed Monte Carlo simulation of a Water Cherenkov Detector (WCD), using CRY-generated sea-level secondaries as inputs to model the detector response to muons, electrons/positrons, photons, and hadrons. It is positioned as a general, experiment-independent reference study for the WCD community. The simulation chain reproduces the key processes governing detector behavior: Cherenkov photon production in water, optical photon transport (including reflections on the inner lining), and conversion to photoelectrons at the photomultiplier tube (PMT). The resulting observables—incident energy, zenith-angle distributions at the detector level, deposited energy, Cherenkov-photon multiplicity (N_{ch}), PMT hit count (N_{hit}), and anode charge (Q)—were constructed with shared logarithmic binning across particle species and analyzed as event counts per bin for direct comparison.

Across all observables, the species-dependent trends are consistent with expectations for a WCD of 1.90 m in height. Muons, with their long above-threshold tracks, dominate

the high tails of the N_{ch}, N_{hit}, and Q spectra. Electrons and photon-induced $e^{\pm}$ pairs populate the low–intermediate energy ranges, contributing substantially to the overall multiplicity. Hadrons, though less abundant at ground level, can deposit significant energy and generate Cherenkov light through above-threshold proton- and neutron-induced charged secondaries and capture gamma rays. The qualitative behavior is consistent with previous experimental observations (e.g., Pierre Auger and HAWC), supporting the realism of the modeled response.

The systematic approach presented here clarifies how particle-dependent track lengths and interaction mechanisms translate into distinct optical and charge signatures in WCDs. Beyond providing a detailed reference for detector response, this framework establishes a transferable foundation for interpreting mixed-particle signals, benchmarking simulation configurations, and guiding the development of particle-identification and background-reduction techniques.

Future work will refine the mapping from optical photons to charge by systematically varying PMT quantum efficiency, gain, and inner-lining reflectivity, as well as by extending the study to array layouts and site-specific atmospheric conditions. The methodology and datasets developed here can be readily adapted by the broader community to address experiment-specific challenges and to support the design and calibration of next-generation WCD-based observatories.

Author Contributions: Conceptualization, L.A.S.P.; methodology, L.A.S.P.; software and validation, L.A.S.P. and R.H.S.; formal analysis, L.A.S.P.; investigation, L.A.S.P.; data curation, L.A.S.P. and R.H.S.; writing—original draft preparation, L.A.S.P. and R.H.S.; writing—review and editing, L.A.S.P.; visualization, L.A.S.P.; supervision, L.A.S.P.; project administration, L.A.S.P.; funding acquisition, L.A.S.P. All authors have read and agreed to the published version of the manuscript.

Funding: Stuani Pereira, L.A. gratefully acknowledges financial support from FAPESP under grant numbers 2021/01089-1, 2024/02267-9, and 2024/14769-9, and from CNPq under grant numbers 403337/2024-0, 153839/2024-4, and 200164/2025-2.

Data Availability Statement: The original contributions presented in this study are included in the article. Further inquiries can be directed to the corresponding authors.

Conflicts of Interest: The authors declare no conflicts of interest.

References

1. Stanev, T. *High Energy Cosmic Rays*, 2nd ed.; Springer Praxis Books, Astronomy and Planetary Sciences; Springer Science & Business Media: Berlin, Germany, 2010.
2. Gaisser, T.; Engel, R.; Resconi, E. *Cosmic Rays and Particle Physics*; Cambridge University Press: Cambridge, UK, 2016; pp. 1–444. [CrossRef]
3. Heck, D.; Knapp, J.; Capdevielle, J.N.; Schatz, G.; Thouw, T. *CORSIKA: A Monte Carlo Code to Simulate Extensive Air Showers*; Forschungszentrum Karlsruhe GmbH: Karlsruhe, Germany, 1998.
4. Engel, R.; Heck, D.; Pierog, T. Extensive Air Showers and Hadronic Interactions at High Energy. *Annu. Rev. Nucl. Part. Sci.* **2011**, *61*, 467–489. [CrossRef]
5. Blümer, J.; Engel, R.; Hörandel, J.R. Cosmic rays from the knee to the highest energies. *Prog. Part. Nucl. Phys.* **2009**, *63*, 293–338. [CrossRef]
6. Etchegoyen, A.; Bauleo, P.; Bertou, X.; Bonifazi, C.; Filevich, A.; Medina, M.; Melo, D.; Rovero, A.; Supanitsky, A.; Tamashiro, A.; et al. Muon-track studies in a water Cherenkov detector. *Nucl. Instrum. Methods Phys. Res. Sect. A Accel. Spectrom. Detect. Assoc. Equip.* **2005**, *545*, 602–612. [CrossRef]
7. Cabrera, R.; Castellina, A.; Ghia, P.; Kakimoto, F.; Kaneko, T.; Morello, C.; Navarra, G.; Nishi, K.; Saavedra, O.; Trinchero, G.; et al. Search for GeV GRBs with the INCA experiment. *Astron. Astrophys. Suppl. Ser.* **1999**, *138*, 599–600. [CrossRef]
8. Falcone for Milagro collaboration, A. Detection of 6 November 1997 ground level event by Milagrito. In Proceedings of the AIP Conference Proceedings, Austin, TX, USA, 10–15 December 2000; American Institute of Physics: College Park, MD, USA, 2000; Volume 510, pp. 574–578.

9. Abraham, J.; Aglietta, M.; Aguirre, I.; Albrow, M.; Allard, D.; Allekotte, I.; Allison, P.; Muniz, J.A.; Do Amaral, M.; Ambrosio, M.; et al. Properties and performance of the prototype instrument for the Pierre Auger Observatory. *Nucl. Instrum. Methods Phys. Res. Sect. A Accel. Spectrom. Detect. Assoc. Equip.* **2004**, *523*, 50–95. [CrossRef]
10. Abeysekara, A.; Aguilar, J.; Aguilar, S.; Alfaro, R.; Almaraz, E.; Álvarez, C.; Álvarez-Romero, J.d.D.; Álvarez, M.; Arceo, R.; Arteaga-Velázquez, J.; et al. On the sensitivity of the HAWC observatory to gamma-ray bursts. *Astropart. Phys.* **2012**, *35*, 641–650. [CrossRef]
11. LHAASO Collaboration. A future project at tibet: The large high altitude air shower observatory (LHAASO). *Chin. Phys. C* **2010**, *34*, 249. [CrossRef]
12. Asorey, H.; Núñez, L.A.; Suárez-Durán, M.; Torres-Nino, L.; Rodríguez-Pascual, M.; Rubio-Montero, A.J.; Mayo-García, R. The latin american giant observatory: A successful collaboration in latin america based on cosmic rays and computer science domains. In Proceedings of the 2016 16th IEEE/ACM International Symposium on Cluster, Cloud and Grid Computing (CCGrid), Cartagena, Colombia, 16–19 May 2016, pp. 707–711.
13. Knoll, G.F. *Radiation Detection and Measurement*; John Wiley & Sons: Hoboken, NJ, USA, 2010.
14. Patrignani, C. Review of Particle Physics. *Chin. Phys. C* **2016**, *40*, 100001. [CrossRef]
15. Aab, A.; Abreu, P.; Aglietta, M.; Ahlers, M.; Ahn, E.J.; Albuquerque, I.; Allekotte, I.; Allen, J.; Allison, P.; Almela, A.; et al. The Pierre Auger Observatory: Contributions to the 33rd International Cosmic Ray Conference (ICRC 2013). *arXiv* **2013**, arXiv:1307.5059. [CrossRef]
16. Hamamatsu Photonics K.K. *Photomultiplier Tubes: Basics and Applications*, 3rd ed.; Hamamatsu Photonics: Hamamatsu City, Japan, 2007.
17. Asorey, H. LAGO: The Latin American Giant Observatory. In Proceedings of the 34th International Cosmic Ray Conference (ICRC2015)—Cosmic Ray Physics: Experimental Results, The Hague, The Netherlands , 30 July–6 August 2015; Sissa Medialab srl Partita: Trieste, Italy, 2016; p. 247. Available online: https://pos.sissa.it/236/247 (accessed on 15 September 2025). [CrossRef]
18. Allard, D.; Allekotte, I.; Alvarez, C.; Asorey, H.; Barros, H.; Bertou, X.; Burgoa, O.; Berisso, M.G.; Martínez, O.; Loza, P.M.; et al. Use of water-Cherenkov detectors to detect gamma ray bursts at the Large Aperture GRB Observatory (LAGO). *Nucl. Instrum. Methods Phys. Res. Sect. A Accel. Spectrom. Detect. Assoc. Equip.* **2008**, *595*, 70–72. [CrossRef]
19. Asorey, H.G. Los Detectores Cherenkov del Observatorio Pierre Auger y su aplicación al Estudio de Fondos de Radiación. Ph.D. Thesis, Universidad Nacional de Cuyo, Mendoza, Argentina, 2012.
20. Sidelnik, I.; Asorey, H.; Guarin, N.; Durán, M.S.; Lipovetzky, J.; Arnaldi, L.H.; Pérez, M.; Haro, M.S.; Berisso, M.G.; Bessia, F.A.; et al. Enhancing neutron detection capabilities of a water Cherenkov detector. *Nucl. Instrum. Methods Phys. Res. Sect. A Accel. Spectrom. Detect. Assoc. Equip.* **2020**, *955*, 163172. [CrossRef]
21. Sidelnik, I.; Asorey, H.; Guarin, N.; Durán, M.S.; Bessia, F.A.; Arnaldi, L.H.; Berisso, M.G.; Lipovetzky, J.; Pérez, M.; Haro, M.S.; et al. Neutron detection capabilities of water Cherenkov detectors. *Nucl. Instrum. Methods Phys. Res. Sect. A Accel. Spectrom. Detect. Assoc. Equip.* **2020**, *952*, 161962. [CrossRef]
22. Watanabe, H.; Zhang, H.; Abe, K.; Hayato, Y.; Iida, T.; Ikeda, M.; Kameda, J.; Kobayashi, K.; Koshio, Y.; Miura, M.; et al. First study of neutron tagging with a water Cherenkov detector. *Astropart. Phys.* **2009**, *31*, 320–328. [CrossRef]
23. Hagmann, C.; Lange, D.; Wright, D. Cosmic-ray shower generator (CRY) for Monte Carlo transport codes. In Proceedings of the 2007 IEEE Nuclear Science Symposium Conference Record, Honolulu, HI, USA, 26 October–3 November 2007; Volume 2, pp. 1143–1146. [CrossRef]
24. Agostinelli, S.; Allison, J.; Amako, K.A.; Apostolakis, J.; Araujo, H.; Arce, P.; Asai, M.; Axen, D.; Banerjee, S.; Barrand, G.; et al. GEANT4—A simulation toolkit. *Nucl. Instrum. Methods Phys. Res. Sect. A Accel. Spectrom. Detect. Assoc. Equip.* **2003**, *506*, 250–303. [CrossRef]
25. Waters, L.S.; McKinney, G.W.; Durkee, J.W.; Fensin, M.L.; Hendricks, J.S.; James, M.R.; Johns, R.C.; Pelowitz, D.B. The MCNPX Monte Carlo Radiation Transport Code. *AIP Conf. Proc.* **2007**, *896*, 81–90. [CrossRef]
26. Usoskin, I.G.; Solanki, S.K.; Krivova, N.A.; Hofer, B.; Kovaltsov, G.A.; Wacker, L.; Brehm, N.; Kromer, B. Solar cyclic activity over the last millennium reconstructed from annual 14C data. *Astron. Astrophys.* **2021**, *649*, A141. [CrossRef]
27. Geant4 Collaboration. *Geant4 Physics Reference Manual*; Geant4 Collaboration: Geneva, Switzerland, 2023. Available online: https://geant4.web.cern.ch/documentation/dev/prm_html/PhysicsReferenceManual/ (accessed on 10 September 2025).
28. Battistoni, G.; Cerutti, F.; Fassò, A.; Ferrari, A.; Muraro, S.; Ranft, J.; Roesler, S.; Sala, P.R. The FLUKA code: Description and benchmarking. In *Hadronic Shower Simulition Workshop*; Albrow, M., Raja, R., Eds.; American Institute of Physics Conference Series; AIP: College Park, MD, USA, 2007; Volume 896, pp. 31–49. [CrossRef]
29. Ostapchenko, S. Monte Carlo treatment of hadronic interactions in enhanced Pomeron scheme: I. QGSJET-II model. *Phys. Rev. D* **2011**, *83*, 014018. [CrossRef]

30. Abeysekara, A.U.; Albert, A.; Alfaro, R.; Alvarez, C.; Álvarez, J.D.; Arceo, R.; Arteaga-Velázquez, J.C.; Ayala Solares, H.A.; Barber, A.S.; Bautista-Elivar, N.; et al. Observation of the Crab Nebula with the HAWC Gamma-Ray Observatory. *Astrophys. J.* **2017**, *843*, 39. [CrossRef]
31. Anderson, M.R.; Andringa, S.; Askins, M.; Auty, D.J.; Barros, N.; Barão, F.; Bayes, R.; Beier, E.W.; Bialek, A.; Biller, S.D.; et al. Measurement of neutron-proton capture in the SNO+ water phase. *Phys. Rev. C* **2020**, *102*, 014002. [CrossRef]

Disclaimer/Publisher's Note: The statements, opinions and data contained in all publications are solely those of the individual author(s) and contributor(s) and not of MDPI and/or the editor(s). MDPI and/or the editor(s) disclaim responsibility for any injury to people or property resulting from any ideas, methods, instructions or products referred to in the content.